Biomedicine & Pharmacotherapy 173 (2024) 116351

Contents lists available at ScienceDirect

Biomedicine & Pharmacotherapy

journal homepage: www.elsevier.com/locate/biopha

Chronic Rapamycin administration via drinking water mitigates the pathological phenotype in a Krabbe disease mouse model through autophagy activation

Ambra Del Grosso [a,b,*], Sara Carpi [a,1], Miriam De Sarlo [a], Luca Scaccini [b], Laura Colagiorgio [a], Husam B.R. Alabed [c], Lucia Angella [a], Roberto Maria Pellegrino [c], Ilaria Tonazzini [a], Carla Emiliani [c], Marco Cecchini [a,*]

[a] Istituto Nanoscienze – CNR, Pisa, Piazza San Silvestro 12, Pisa 56127, Italy
[b] Laboratorio NEST, Scuola Normale Superiore, Piazza S. Silvestro 12, 56127, Pisa, Italy
[c] Department of Chemistry, Biology, and Biotechnologies, University of Perugia, Perugia, Italy

ARTICLE INFO

Keywords:
Krabbe disease
Globoid cell leukodystrophy
autophagy induction
Rapamycin
psychosine
Twitcher mouse
P62aggregates

ABSTRACT

Krabbe disease (KD) is a rare disorder arising from the deficiency of the lysosomal enzyme galactosylceramidase (GALC), leading to the accumulation of the cytotoxic metabolite psychosine (PSY) in the nervous system. This accumulation triggers demyelination and neurodegeneration, and despite ongoing research, the underlying pathogenic mechanisms remain incompletely understood, with no cure currently available. Previous studies from our lab revealed the involvement of autophagy dysfunctions in KD pathogenesis, showcasing p62-tagged protein aggregates in the brains of KD mice and heightened p62 levels in the KD sciatic nerve. We also demonstrated that the autophagy inducer Rapamycin (RAPA) can partially reinstate the wild type (WT) phenotype in KD primary cells by decreasing the number of p62 aggregates. In this study, we tested RAPA in the Twitcher (TWI) mouse, a spontaneous KD mouse model. We administered the drug *ad libitum* via drinking water (15 mg/L) starting from post-natal day (PND) 21–23. We longitudinally monitored the mouse motor performance through grip strength and rotarod tests, and a set of biochemical parameters related to the KD pathogenesis (i.e. autophagy markers expression, PSY accumulation, astrogliosis and myelination). Our findings demonstrate that RAPA significantly enhances motor functions at specific treatment time points and reduces astrogliosis in TWI brain, spinal cord, and sciatic nerves. Utilizing western blot and immunohistochemistry, we observed a decrease in p62 aggregates in TWI nervous tissues, corroborating our earlier in-vitro results. Moreover, RAPA treatment partially removes PSY in the spinal cord. In conclusion, our results advocate for considering RAPA as a supportive therapy for KD. Notably, as RAPA is already available in pharmaceutical formulations for clinical use, its potential for KD treatment can be rapidly evaluated in clinical trials.

1. Introduction

Krabbe disease (KD) or Globoid cell leukodystrophy is a rare genetic disease (OMIM: 245200), with a prevalence of 1–9/100000 [14]. It is caused by mutation occurring in homozygosis or in compound heterozygosis into the GALC gene, which encodes for the lysosomal enzyme galactosylceramidase (GALC; EC 3.2.1.46) [27]. GALC deficiency causes increased of levels of the cytotoxic D-galactosylsphingosine [psychosine

Abbreviations: KD, Krabbe disease; GALC, galactosylceramidase; PSY, psychosine; RAPA, Rapamycin; WT, wild type; TWI, Twitcher; PND, post-natal day; ERT, enzyme replacement therapy; LC3, microtubule-associated protein 1 light-chain 3; ATG5, autophagy-related 5; P62, ubiquitin-binding protein p62; PNS, peripheral nervous systems; CNS, central nervous system; HET, heterozygous; TP, time points; TWI+RAPA, Twitcher mice treated with Rapamycin; BCA, micro-bicinchoninic acid; LC/HRMS, High-Resolution Mass Spectrometry, PFA, paraformaldehyde; RT, room temperature; BSA, bovine serum albumine; SDS-PAGE, Sodium Dodecyl Sulfate Polyacrylamide Gel Electrophoresis; MBP, myelin binding protein, GFAP, glial fibrillary acidic protein; HPR, horseradish peroxidase; GAPDH, glyceraldehyde 3-phosphate dehydrogenase; DMEM, Dulbecco's modified eagle medium; FCS, fetal calf serum; ITI, inter-trial interval.

* Corresponding authors at: Istituto Nanoscienze – CNR, Pisa, Piazza San Silvestro 12, Pisa 56127, Italy.
E-mail addresses: ambra.delgrosso@sns.it, ambradelgrosso@cnr.it (A. Del Grosso), marco-cecchini@cnr.it (M. Cecchini).
[1] Present Address: Department of Health Sciences, University 'Magna Græcia' of Catanzaro, 88100 Catanzaro, Italy.

https://doi.org/10.1016/j.biopha.2024.116351
Received 1 December 2023; Received in revised form 17 February 2024; Accepted 23 February 2024
Available online 28 February 2024

(PSY)] in neural tissues, leading to widespread degeneration of oligodendrocytes and Schwann cells and subsequent deadly demyelination [24]. The most frequent KD form is the early infantile one, (95% of known cases), whose onset is typically within the first 6 months of life and leads to death by 2 years of age [73]. Currently bone marrow transplantation is the only clinically applied method to treat KD, but unfortunately it has shown some success only in infants who are treated before the onset of symptoms and in some older children and adults [18,47]. On the other end, gene therapy has yielded good results in several experimental models [41]. Two clinical trials based on gene therapy are currently ongoing to test the efficacy of GALC gene delivery through adeno-associated vector into KD patients (FBX-101 and PBKR03; ClinicalTrials.gov Identifier: NCT04693598 and NCT04771416). Interesting results in KD *in-vitro* and *in-vivo* models have also been published regarding enzyme replacement therapy (ERT) mediated by nanovectors [9,10,13,23,61].

Despite these efforts, however, the literature suggests that restoring GALC activity up to the level of unaffected organisms might be not enough to completely rescue the KD phenotype [26,52,58]. Thus, the idea has emerged that supplementary therapies addressing secondary alterations resulting from GALC dysfunction at early stages [19] might be needed to improve the final therapeutic result. [3,57]

However, achieving this goal remains difficult because the molecular pathogenesis of KD has not yet been completely elucidated.

For the most widely accepted theory (the "PSY-hypothesis"), PSY acts as a detergent which disrupts membrane microdomain organization of lipid rafts, thereby causing cell death [25,67,74]. Accordingly, PSY can trigger apoptosis in KD oligodendrocyte progenitors by inducing activation/cleavage of initiator caspase-8 and −9, and effector caspase-3. [75] Furthermore, PSY has been proposed to cause α-synuclein formation and neurodegeneration in KD tissues [65]. Therefore, the proposed mechanisms for PSY-induced toxicity are broad and multifaceted, and much question remains open [19]. Recent discoveries support the hypothesis that some molecular pathogenetic mechanisms in KD cells occur independently from PSY, such as endothelial cell dysfunction [2], or mechanotransduction impairment [40].

Recently, we demonstrated the involvement of autophagy dysfunctions in KD pathogenesis, *in in-vitro* and *in-vivo* KD models. [11,12,15,40,49] The autophagy pathway degrades cytosolic material, such as damaged organelles, proteins, carbohydrates, and lipids, by delivery to the lysosome. It begins with the formation of double-membrane vesicles called autophagosomes from cup-shaped structures called phagophores. At this point, the microtubule-associated protein 1 light-chain 3 (LC3) helps fold phagophore edges and binds adapter proteins (such as the ubiquitin-binding protein p62) that promote the degradation of specific cellular and molecular structures. The autophagosome then fuses with the lysosome to form the autolysosome, where the resident hydrolases degrade the luminal material. [53]

Basically, in KD we showed a dysregulation at the level of the main autophagy markers: LC3, p62, Beclin-1 and the autophagy-related 5 (ATG5). [12,49] We found p62-tagged protein aggregates in the brain of KD mice and increased p62 levels in the KD sciatic nerve, suggesting the inability of the KD cells to dispose-off all the p62-tagged – "waste materials", and indicating a possible engulfment of the autophagy flux in KD. [12,36] We also demonstrated that the autophagy inducer Rapamycin (RAPA) can partially reinstate the wild type (WT) phenotype in KD primary cells by decreasing the number of p62 aggregates. [12] Autophagy deregulations in KD have been also confirmed by other groups, including Ribbens et al., [56], Lin et al. [36], Rebiai et al. [54], and Papini et al. [48]. In particular, Ribbens and colleagues demonstrated increased levels of LC3-B in a novel disease cell model of KD, speculating that it may be a part of the autophagy process or a result of a disruption in the autophagy flow caused by the impairment of the lysosomal system due to primary GALC deficiency [56]. Later, Rebiai and collaborators demonstrated a decreased autophagosome/lysosome fusion in cultured neural precursors derived from two novel mouse models for KD, which recapitulate the early- and adult-onset forms of the disease [54]. Interestingly, Papini et al. [48] recently demonstrated that inhibitory AKT-mediated phosphorylation of beclin-1 and the BCL2-beclin-1 complex contribute to the reduction of autophagosome formation in response to starvation in fibroblasts isolated from patients, independently of PSY accumulation.

With this study, we decided to test RAPA *in-vivo* to evaluate its capability to remove unwanted cellular products specific of KD, such as p62 aggregates and PSY. We tested RAPA on the Twitcher (TWI) mouse, which is a spontaneous KD mouse model [31]. The drug was administered *ad libitum* via drinking water (15 mg/L) starting from post natal day (PND) 21–23, which is the age of symptom onset in TWI mice [17], and continued until sacrifice. We longitudinally monitored the mice body weight (BW) and motor performances through the grip strength and rotarod tests. We also assayed a set of biochemical parameters related to the KD pathogenesis (i.e. autophagy markers expression, PSY accumulation, astrogliosis and myelination) after treatment in both the CNS and the peripheral nervous systems (PNS).

2. Materials and methods

2.1. Chemicals materials

Deuterated Psychosine Quantitative Mass Spec Standard (Galactosyl (β) Sphingosine-d5; PSY-d5) was purchased from Avanti Polar Lipids. Water, Acetonitrile, Isopropanol and Methanol LC/MS grade, Chlorophorm, Ammonium Acetate and Ammonium Fluoride were purchased from Sigma Aldrich.

2.2. Animal procedures

Twitcher heterozygous (HET) mice (TWI+/− C57BL6 mice; the Jackson Laboratory, Bar Harbor, ME), generously provided by Dr. Biffi (San Raffaele Telethon Institute for Gene Therapy, Milan, Italy), were used as breeder pairs to generate homozygous TWI mice (TWI−/−, elsewhere in the paper abbreviated as TWI for simplicity) at the Center for Experimental Biomedicine of CNR, in Pisa. The animals were maintained under standard housing conditions and used according to the protocols and ethical guidelines approved by the Ministry of Health (permit no. 535/2018-PR; official starting date: 9 July 2018). As previously conducted by our group [1,13], genomic DNA was extracted from tail clippings of PND 10–15 mice using the EUROGOLD Tissue-DNA Mini Kit from EUROCLONE. The genetic status of each mouse was determined by analyzing the TWI mutation using a fast real-time PCR-based protocol recently developed in our laboratory [6,7]. TWI and wild type (WT) animals were used for the experiments [experimental groups: untreated WT (WT); untreated TWI (TWI); Rapamycin (RAPA) - treated TWI (TWI+RAPA)]. We used 4 mice for the WT group, 4 mice for the TWI group, and 6 mice for the TWI+RAPA group. Starting from PND 21–23, mice received chronic Rapamycin (RAPA) dissolved in their drinking water at a concentration of 15 mg/L, a dosage previously shown to induce a significant concentration in the mice serum. [28,35,46,60,63]. Mice were treated until they reached a body weight loss of ≥25% (for a total of 17–19 day of treatment), which was the chosen ethical endpoint. At this point, they were euthanized (WT mice, on the other hand, were euthanized along with the last sacrificed TWI mouse in the specific experiment). Mice underwent behavioral tests at three time points (TP): TP 1 = PND 24–25; TP 2 = PND 29–30; TP 3 = PND 35–37. Refer to Fig. 1 A for a graphical depiction of the experiment's timeline. At the end of the experiment, the mice were deeply anesthetized with a urethane solution (0.8 ml/g; Sigma-Aldrich) and then euthanized by decapitation. Subsequently, tissues were extracted from each mouse processed. All procedures were performed with the utmost effort to minimize the suffering of the mice.

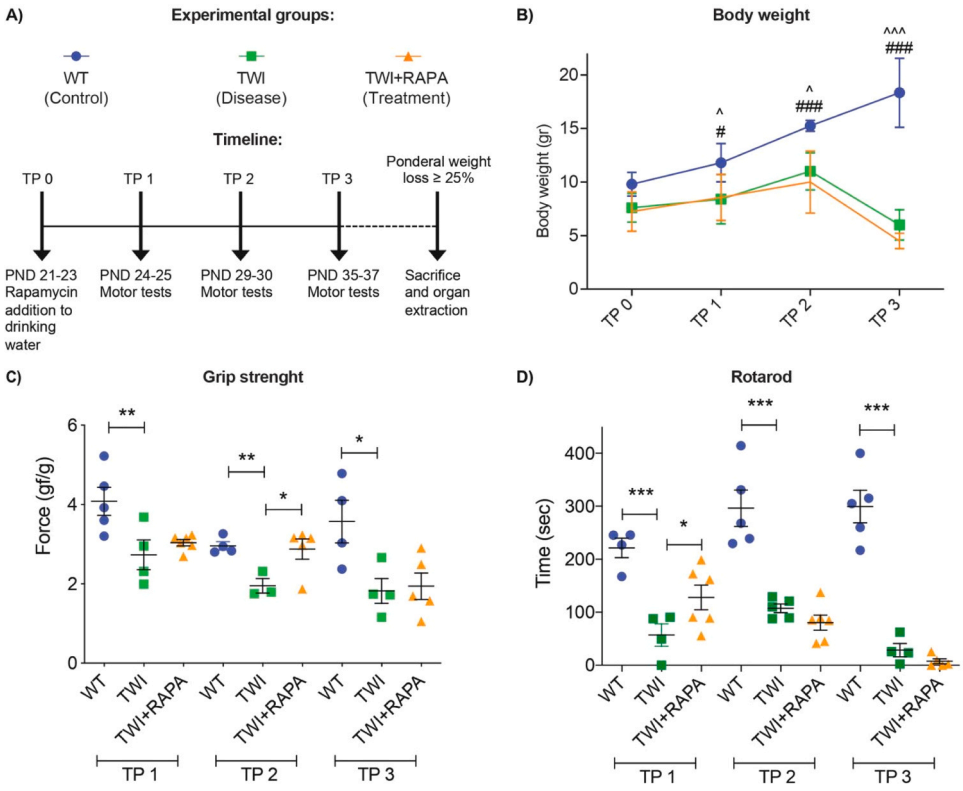

Fig. 1. Administration of Rapamycin by drinking water in Twitcher (TWI) mice. A) Experimental design. Rapamycin (15 mg/L) has been administered via drinking water ad libitum to TWI mice, starting at post-natal day (PND) 21–23 [Time point 0 (TP 0) of the experiments] until mouse sacrifice (i.e. when ponderal weight loss ≥ 25%). As control, we used untreated Wilde Type (WT) and TWI mice. Motor tests (grip strength test and rotarod test) were carried out on treated (TWI+RAPA) and untreated (WT, TWI) mice at 3 TPs (TP 1 = 24–25, TP 2 = 29–30, and TP3 = 35–37). B) Body weight (BW) measured in grams. # P <.05, ### P <.01 TWI vs. WT; ^ P <.05, ^^^ P <.01 TWI+RAPA vs. WT. N = between 5 and 9 mice for each experimental group. C-D) RAPA treatment effects on TWI mice motor performances. Legend: WT = blue circles, TWI = green square, TWI-Li = orange triangle. C) Grip strength test. Data are normalized on the mice's body weight and reported in the graph in gram-force/gram (gf/g). * P <.05, ** P <.01 TWI vs. WT or TWI+RAPA vs. TWI D) Rotarod test. Data are reported in the graph in seconds (s). * P <.05, *** P <.001 TWI vs. WT or TWI+RAPA vs. TWI. B-D) Data are reported as mean ± SEM and compared using the One way ANOVA (Bonferroni's test). N = between 4 and 6 mice for each experimental group.

2.3. Motor behavioral experiments

We conducted motor behavioral experiments (grip strength and rotarod tests) [4], at the three time points mentioned above. The experiments involved three experimental groups: untreated WT, untreated TWI, and TWI mice treated with RAPA (TWI+RAPA). Additionally, the body weight of the mice was measured at each time point.

2.3.1. Rotarod test

We used a rotarod apparatus (Ugo Basile) to assess motor coordination skills, as previously described [Del Grosso et al., 2021]. The rotarod apparatus consists of five 3 cm diameter cylinders, each machined to provide grip. It is divided into five lanes, each 5.7 cm wide, allowing up to five mice to be on the rotor simultaneously. Mice were placed on the horizontally suspended rotating rod, 16 cm above the floor, and underwent four trials per day with a 15-minute inter-trial interval (ITI). The cutoff speed was set at 4 rpm, with a maximum trial duration of 5 minutes. The mean latency to fall was calculated for each animal.

2.3.2. Grip strength test

Mice were positioned on a base plate in front of an adjustable-height grasping bar (trapezoid-shaped) as previously described [14,71]. The bar was equipped with a force transducer connected to a Peak Amplifier (Ugo Basile). When the mice were pulled by their tails, they instinctively gripped the bar until the pulling force exceeded their grip strength. Once the animal released its grip on the bar, the peak amplifier automatically recorded the peak pull-force achieved by the forelimbs and displayed it on a liquid crystal display. Each animal underwent three trials per day with a 15-minute inter-trial interval, and the average pull-force was calculated. For both motor behavioral experiments, groups of 4–7 mice were tested, and the data is presented as the mean ± standard error of the mean (SEM).

2.4. Mice organs processing

Tissues (total brain, cerebrum, cerebellum, spinal cord, sciatic nerves, liver and kidneys) were extracted from each mouse and immediately put on 1.5 ml microcentrifuge tubes on ice. Tubes were previously put on ice with distinct volumes of RIPA buffer (R0278; Sigma Aldrich), depending on the organ (1000 µl for the total brain or cerebrum; 300 µl for the cerebellum; 200 µl for the spinal cord, 100 µl for the sciatic nerves, 500 µl for liver and 300 µl for kidneys). RIPA buffer was previously prepared with both a protease and phosphatase inhibitors cocktail [cOmplete (4693116001) and PhosSTOP (4906845001); Roche Diagnostics]. Organs were then homogenized on ice with pestles, centrifuged (15.000 g for 30 minutes, at 4 °C) and tested for protein concentration by the micro-bicinchoninic acid (BCA) Protein Assay Kit (Thermo Scientific Pierce). The BCA assay was done using 1 µl of the organ lysate diluted in 100 µl of sterile distilled water, in 96 well plates. Each sample was assayed in duplicate. Absorbance (562 nm) was read by using the GloMax® Discover Microplate fluorescence reader (Promega). Organs lysates were stored at −80 °C.

2.5. Psychosine quantification

PSY quantification was assessed on homogenate samples after a lipid extraction step, using Liquid Chromatography coupled with High-Resolution Mass Spectrometry (LC/HRMS), as previously done. [1,14,40] The extraction was carried out according to the method described by Fuller M. *et al.*, [22] with minor modifications. Briefly, each homogenate sample (12–100 μL) was diluted 4 times with a mixture of 1:2 of Chloroform/Methanol containing the PSY-d5 as Internal Standard at the concentration of 200 ng/ml. Samples were mixed for 20 minutes on a thermomixer (Euroclone T-Shaker) at 1700 rpm and at room temperature. Afterwards, proteins were sedimented by centrifugation at 13,000 rpm for 10 min ad 4 °C. The supernatant was transferred into glass autosampler vials and immediately subjected to LC/HRMS analysis. A lipidomic liquid chromatography method [32] was used to achieve a wide separation of PSY from other lipid molecular species. Quantitative data were obtained by injecting 20 μL of extract samples on an Agilent 6530 Q-TOF LC/MS (Agilent Technologies, Inc., Santa Clara, CA, USA), by Data Dependent Acquisition. Acetate adducts of natural PSY and PSY-d5 were monitored in negative ionization mode with accuracy within ± 2.5 ppm. The peak area was used for quantification. PSY concentration was expressed as pg/μg of protein and reported as a percentage of the mean TWI cerebrum value.

2.6. Immunohistochemistry

WT, TWI and TWI+RAPA deeply anaesthetized mice were sacrificed by transcardiac perfusion with phosphate buffer saline (PBS) and subsequently with paraformaldehyde (PFA) 4%. After perfusion, brains were stored at 4 °C in a 4% PFA solution for a minimum of 2 days. Consecutive coronal brain sections, 60 μm thick, were cut with a vibratome (Leica VT1000 S) at 0.50–2.10 mm from bregma. Sections were maintained at 4°C in PBS until use. For the immunohistochemistry staining, sections were transferred in a 24-well cell culture plate (maximum of 3 sections per well) and incubated with blocking solution (3% bovine serum albumin, 0.3% TritonX-100 in PBS; 1 ml per well) for 1 hour at room temperature (RT). Then, the blocking solution was removed and the primary antibody mix (1% BSA, 0.3% TritonX-100, antibody at the optimal dilution and PBS to reach 1 ml) was added to the well and left overnight at 4° under gentle shaking. We used the following antibodies: anti-p62 (ab56416 Abcam, 1:100), anti-LC3 (ab48394 Abcam, 1:200), anti-GFAP (ab7260 Abcam, 1:1000), anti-MBP (ab980 Merck Millipore, 1:500), anti-Ubiquitin (1:200, rabbit, Proteintech #10201–2-AP). These primary antibodies have been validated in previous studies [11,20,21,38,66]. Next morning, the primary antibody solution was removed and 3 washes with 1 ml of PBS were made (10 minutes each). Then, the secondary antibody solution was added (BSA 1%, TritonX-100 0,3%, anti-mouse or anti-rabbit Alexa 647 1:1000, anti-mouse or anti-rabbit Alexa 488 1:000 and PBS to reach 1 ml total volume). After 2 hours of incubation at room temperature, three additional washes with PBS were performed. Sections were then stained with a Hoechst solution for 1 minute and then mounted on SUPERFROST Microscope Slides (Thermo Scientific) with Vectashield Antifade Mounting Medium (VECTOR LABORATORIES). Finally, slides were sealed and stored at 4 °C until confocal imaging.

2.7. Confocal microscopy and images analysis

Immunostained brain sections were imaged with a laser scanning confocal microscope TCS SP2 (Leica Microsystems) equipped with a 63X oil objective and interfaced with UV, Ar, HeNe and He lasers for excitation at 405, 488, 561 and 633 nm, respectively. Each reported confocal image was obtained from a z-series (stack depth was maximum 10 μm with steps of 0.5–1 μm for cells and maximum 20–30 μm with steps of 2 μm for brain sections). The resulting z-stack was processed in ImageJ (NIH; RRID:SCR_003070) into a single image by using "z-project" and "Max intensity" options. The processed z-stack was then merged using the "Merge channel options". For the quantitative analysis of the p62 aggregates, the procedure was conducted as previously described in our prior study [12]. Briefly, every image was thresholded using the "threshold" tool and the number of particles was analysed by the "Analyze Particles" plugin, by setting "size (micron^2)" = from 1 to infinity for p62 analysis and from 10 to infinity for astrocytes analysis, and "circularity" = from 0.00 to 1.00. For each graph, images were taken with the same magnification. The confocal settings were kept the same, with pinhole aperture set at 1.0 Airy level and 512 ×512 pixels image format for all the experiments. The scale bars for Figs. 2, 4, and 6 are set at 37 μm, while the scale bar for Fig. S1 is 6 μm. Figs. 2 and 4 display images at 6X zoom.

2.8. Immunoblotting

Western blot was carried out on tissue lysates (cerebrum, spinal cord and sciatic nerves), processed as previously described, and stored at −80 °C. Samples were thawed and boiled in Laemmli buffer containing β-mercaptoethanol (5% final concentration) for 5 minutes, centrifuged at room temperature and the supernatants were finally used for gel electrophoresis (SDS-PAGE) or kept at −80 °C until use. 15 μg of brain lysates and 5 μg of spinal cord or sciatic nerves lysates were resolved by SDS-PAGE using Gel Criterion XT-Precast polyacrylamide gel 4–12% Bis-Tris (3450123; Bio-Rad) and subsequently transferred to nitrocellulose membranes as previously described. [11,12] Immunodetection was performed with the following primary antibodies: anti-LC3 (1:1000, rabbit, ab48394 Abcam), anti-p62 (1:800, mouse, ab56416 Abcam), anti- myelin binding protein (MBP) (1:1000, mouse, Abcam 62631), anti- Glial Fibrillary Acidic Protein (GFAP) (1:1000, mouse, Synaptic System 173211BT). On the following day, the membranes were incubated with the corresponding peroxidase-linked secondary antibodies (goat anti-rabbit or mouse IgG- horseradish peroxidase (HRP) conjugate; 1:2500–1:3000, Bio-Rad #1706516 and 1706515) and developed with Clarity enhanced chemiluminescent substrates (Bio-Rad #1705061). The chemiluminescent signal was acquired with an ImageQUANT LAS400 scanner (GE Healthcare Life Science), and the density of immunoreactive bands was quantified by ImageJ (NHI). For GFAP western blot was quantified the upper band, for MBP western blot both bands were quantified togheter. The membranes were then incubated with a stripping buffer containing β-mercaptoethanol (62.5 mM Tris-HCl pH 6.8, 2% SDS, 100 mM 2-Mercaptoetanolo) and re-incubated as above with anti-tubulin (1:3000, mouse, Sigma-Aldrich #T6074) or anti- glyceraldehyde 3-phosphate dehydrogenase (GAPDH) (1:3000, mouse, Sigma-Aldrich #G8795) antibody, and then processed as above. The results were normalized to the tubulin, or GAPDH content for each organ lysate and reported as a percentage in respect to the WT untreated condition.

2.9. Cell culture and treatments

Adult mouse fibroblast cultures were obtained from WT and TWI ears, according to the protocol established in the laboratory of Dr Evan Eichler (University of Washington, https://genome.ucsc.edu/ENCODE/protocols/cell/mouse/Fibroblast_Stam_protocol.pdf) from mice that were less than six months old, as described in our published papers [13,40]. Briefly, after anaesthesia, mouse ears were extracted, washed with sterile water and cut into small pieces. All pieces were collected in an Eppendorf tube and added with collagenase XI (C7657–100 mg; Sigma Aldrich) diluted in high glucose Dulbecco's Modified Eagle Medium (DMEM) (approximately 2.5 mg of collagenase −320 CDU- for 1 mouse). After 2 hours of incubation at 37 °C the Eppendorf tube was centrifuged for 5 minutes at 200 g, the supernatant was discarded and the pellet was washed with 2 ml of PBS and centrifuged again discarding the supernatant. Trypsin-EDTA 0.05% (59418 C-100 ml; Thermo Fisher Scientific) was then added to the tube and left for 45 minutes at 37 °C.

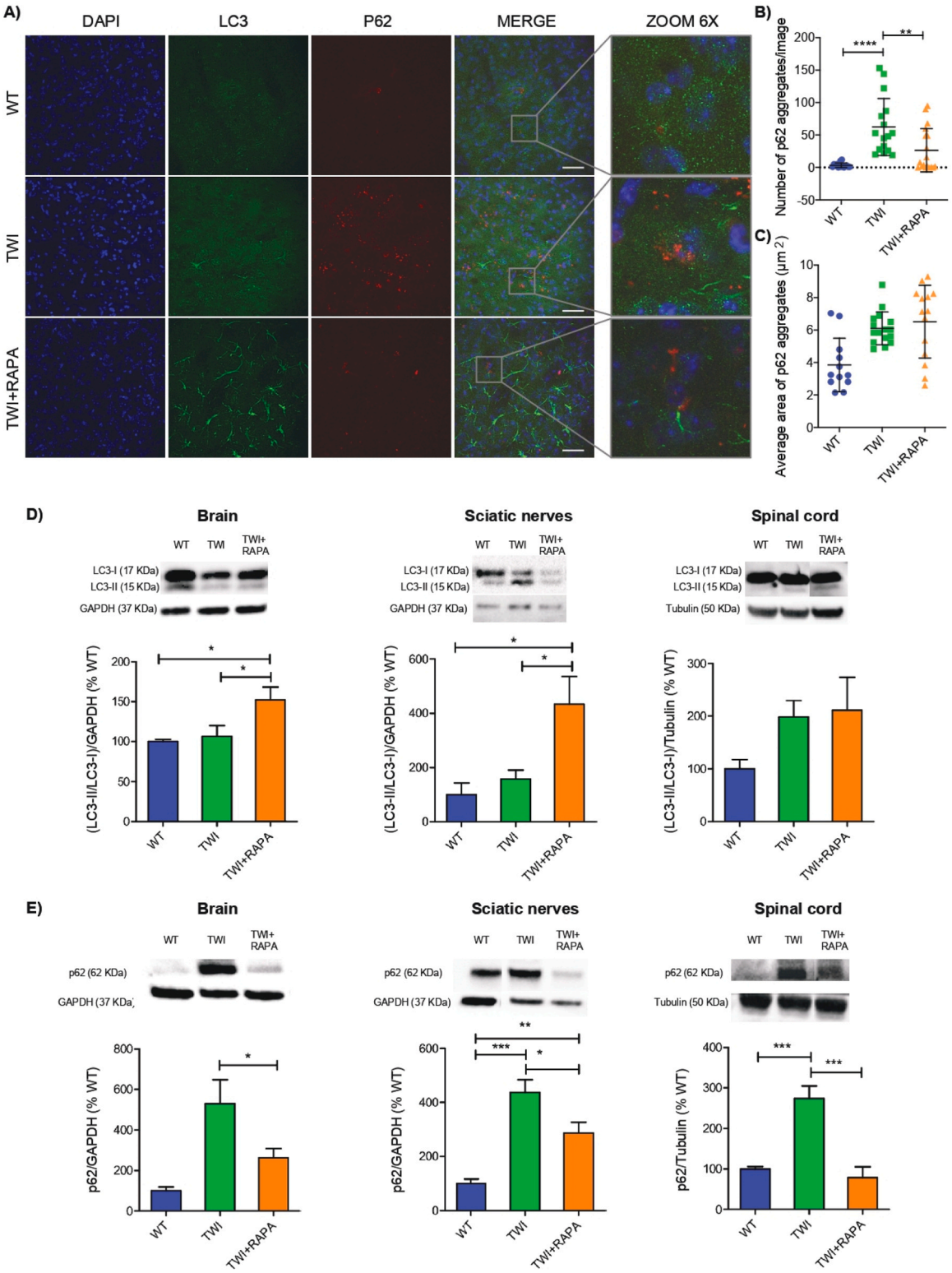

Fig. 2. Rapamycin-mediated autophagy activation in TWI mice nervous system. A) Immunohistochemistry staining of WT, TWI and TWI+RAPA brains with anti-p62 (in red) and anti-LC3 (in green) antibodies, nuclei are stained with DAPI (in blue). A 6 X zoom is shown in the right part of the figure for each merged image. Scale bar: 37 µm. B-C) Analysis of the number and average area of p62 puncta per imaging field. B) p62 puncta: **** $P < 0.0001$, ** $P < 0.01$, TWI+RAPA vs. TWI, TWI vs. WT. C) Average area of p62 puncta (µm2). Data are reported as mean ± SD, and compared using One way ANOVA (Tukey's multiple comparisons test). N = between 15 and 18 images for each group. D-E) Western blot analysis of the total autophagy-related protein light chain 3 (LC3)-II and sequestosome1/p62 (p62) content in whole brain, sciatic nerves and spinal cord lysates of RAPA treated (TWI+RAPA) and untreated (WT, TWI) mice. Representative western blot bands are reported above each graph. N = between 3 and 6 mice for each experimental group. * $P < .05$, *** $P < .001$ TWI vs. WT; TWI+RAPA vs. WT, TWI+RAPA vs. TWI. Data are reported as mean ± SEM, normalized to the total Tubulin or GAPDH content, and compared using One way ANOVA (Bonferroni's test). Western blot data are reported as percentage vs. WT values.

The tube was than centrifuged and the pellet was resuspended in the complete DMEM [high glucose DMEM supplemented with 10% of heat-inactivated fetal calf serum (FCS), 4 mM L-glutamine, 1% MEM Nonessential Amino Acids and 1% penicillin/streptomycin; all products were from GIBCO-Life Technologies)]. Obtained cells were thus divided pipetting up and down with a syringe, plated in a 60 mm cell petri and incubated at 37 °C in a humidified atmosphere containing 5% CO_2. The day after, cells were washed and the medium was replaced. When reaching confluence (approximately 3–4 days), p0 cells were washed with 1 ml of PBS and split with a 1:2 ratio. Cells were cultured and used for experiments within the 10th passage *in vitro*. For treatments, WT and TWI fibroblast primary cells were plated in standard 96-well cell plates (4000 cells per well). After 24 hours, depending on the treatment, cells were pre-treated with RAPA 100 nM (tlrl-rap 5 mg; InvivoGen) for 1 hour and then administered with PSY 100 μM (P9256–1MG; Sigma Aldrich). PSY and RAPA were dissolved in dimethylsulfoxide (DMSO). Control cultures received the same quantity of DMSO, which never exceeded 0.6% v/v. For viability measurements, we employed the 2-(2-methoxy-4-nitrophenyl)-3-(4-nitrophenyl)-5-(2,4-disulfophenyl)-2 H-tetrazolium monosodium salt (WST-8) assay, following the manufacturer's instructions (Sigma, #96992; [59]). Cells were incubated in a 10% WST-8 solution (in DMEM) for 3 hours in the cell incubator at 24, 72, and 96 hours post-treatment. Subsequently, the supernatant was transferred to a new plate, and the absorbance of each well was measured at 450 nm using a GloMax DISCOVER plate reader (Promega).

2.10. Statistical analysis

Unless otherwise specified, data are presented as mean ± SEM or SD, derived from a minimum of three independent samples/experiments. In figure legends, 'N' indicates the number of samples/experiments conducted. Statistical analysis was performed using Prism 6.00 (GraphPad Software, San Diego, CA; RRID: SCR_002798). Parametric data were analyzed using one-way ANOVA with Bonferroni correction for selected pairs; it was assumed that the mean values obtained in each repeated experiment were normally distributed around the true mean. Statistical significance refers to results with a P-value < 0.05.

3. Results

3.1. Rapamycin administration by drinking water improves the motor function of TWI mice at selected time points

We treated Twitcher mice with Rapamycin (RAPA) administered at the concentration of 15 mg/L in the drinking water *ad libitum*, from PND 21–23 [time point (TP) 0]. We tested untreated Wild Type (WT) mice, untreated Twitcher (TWI) mice, and TWI mice treated with RAPA (TWI+RAPA) for their motor abilities at three-time points (TP 1 = PND 24–25; TP 2 = PND 29–30; TP 3 = PND 35–37). See Fig. 1 A for a graphical description of the timeline of the experiments and the section "Material and Methods" for further details. To evaluate the BW increase/decrease with respect to the first day of treatment, we measured it at each TP. The BW of TWI mice did not show the physiological increase found for WT mice already at TP 1 (PND 24–25), as expected. Then, from TP 3 until sacrifice (occurring when mice reached a ponderal weight loss $\geq$ 25%), both TWI and TWI+RAPA mice progressively lost BW (Fig. 1 B) with a similar trend.

To evaluate the neuromuscular function, we performed the grip strength test. As expected, WT mice presented a significantly higher force of the forelimbs with respect to TWI at all tested TP (Fig. 1 C). TWI+RAPA mice presented a force comparable to TWI at TP 1 and 3. Interestingly, at TP 2 (PND 29–30), TWI+RAPA mice exhibited greater strength compared to TWI, with force values closer to those of the WT (P value < 0.05 TWI-RAPA vs. TWI, One-way ANOVA). By the rotarod test, we finally evaluated motor coordination (Fig. 1 D). RAPA led to some improvement at TP 1. At this time point, indeed, TWI+RAPA mice performed slightly better than untreated TWI mice (P value < 0.05 TWI-RAPA vs. TWI, One way ANOVA). At TP 2 and 3, instead, this difference disappeared, and TWI-RAPA and TWI behaved significantly worse than WT mice.

During these experiments, we also monitored some general mouse welfare parameters: food and water consumption, interaction with peers, normal respiration and provoked pattern of behaviour, tremors, prostration, and self-mutilation. In general, we did not observe any deterioration of these parameters (data not shown), demonstrating a good tolerance of the mice to our treatment protocol.

Overall, we thus found that RAPA administration in drinking water can transiently improve the motor function of TWI mice.

3.2. Rapamycin treatment promotes the clearance of p62-tagged aggregates in the nervous system of TWI mice by autophagy activation

To investigate the effect of RAPA administration on the autophagy pathway we examined the expression of the proteins LC3 and p62 in the brain, sciatic nerves, and spinal cord. By immunocytochemistry we found a higher expression of LC3 in brain slices of TWI+RAPA mice with respect to TWI and WT, suggesting that the RAPA treatment could activate the autophagy flux (Fig. 2 A). Accordingly, the western blot analysis we performed on total brain lysates revealed a higher expression of the ratio LC3-II/LC3-I in TWI+RAPA mice compared to TWI and WT (Fig. 2 D). Being the conversion of LC3-I into LC3-II a fundamental step for autophagosome formation [42], these findings confirmed RAPA-mediated autophagy activation. The same trend of LC3-II/LC3-I was present also in both sciatic nerves and spinal cord, indicating autophagy activation also in these organs (Fig. 2C).

As already reported by us and others [12,37], we measured a higher amount of p62-tagged protein aggregates in the brain of TWI mice compared to WT (P value <.001 TWI vs. WT, One way ANOVA; Fig. 2 A-B). Interestingly, the number of p62-aggregates resulted significantly reduced in TWI+RAPA mice compared to TWI (P value <.01 TWI-RAPA vs. TWI; One way ANOVA, Fig. 2 A-B), revealing that RAPA can promote p62-tagged protein aggregates clearance in the TWI mouse brain. The average area of aggregates was instead the same for WT, TWI and TWI+RAPA mice (Fig. 2 C). Western blot data confirmed the immunocytochemistry findings, demonstrating a reduction of the total p62 content in whole brain lysate of TWI+RAPA mice compared to TWI (P value <.05 TWI-RAPA vs. TWI, One way ANOVA; Fig. 2 E). The same trend is maintained in sciatic nerves and spinal cord (Fig. 2 E), confirming the ability of RAPA in promoting p62 clearance also in these organs. Noteworthy is the fact that the reduction is more pronounced in the spinal cord with respect to the other tested organs (P value <.001 TWI-RAPA vs. TWI; One way ANOVA). Finally, in accordance with the western blot data recently published by Lin and colleagues [37], we found that p62 aggregates colocalize with Ubiquitin in the brain of TWI+RAPA-treated mice (Fig. S1).

3.3. Rapamycin treatment enhances PSY removal in TWI spinal cord

To evaluate the efficacy of RAPA in facilitating PSY removal from the TWI nervous system, PSY content in TWI cerebrum, sciatic nerves, spinal cord, and cerebellum was quantified utilizing Liquid Chromatography coupled with High-Resolution Mass Spectrometry (LC/HRMS).

As expected, we detected negligible PSY in the organs of WT animals [Fig. 3 A-B-C-D; [14,39]]. In the cerebrum, sciatic nerves, and cerebellum, there was no significant difference in PSY accumulation between TWI and TWI+RAPA groups (Fig. 3 A-B-D). Instead, a substantial reduction in PSY content was observed in the spinal cord of TWI+RAPA mice compared to untreated TWI mice, demonstrating the efficacy of RAPA in promoting PSY removal within this organ (see Fig. 3 C). Additionally, PSY levels were assessed in major accumulation organs. Consistent with prior studies [8,29,58], PSY concentrations in the liver

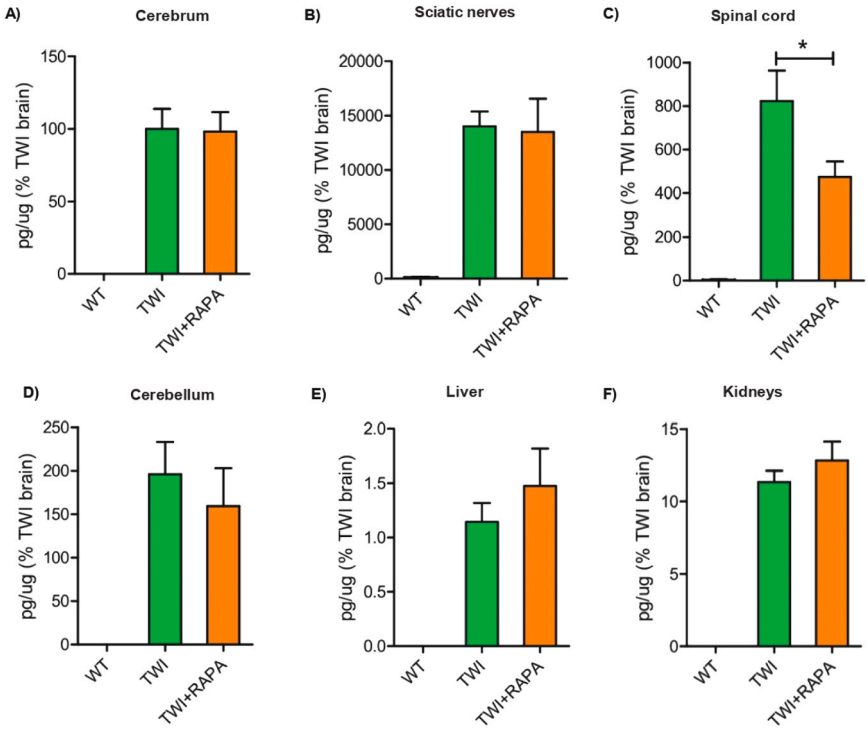

Fig. 3. Psychosine (PSY) content in Rapamycin-treated TWI mice. A-F) HPLC/MS quantification of PSY content in lipid fraction extracted from whole cerebrum, sciatic nerve, spinal cord, cerebellum, liver, and kidneys lysates of RAPA-treated (TWI+RAPA) and untreated (WT, TWI) mice. F) Spinal cord: * P <.05 P TWI+RAPA vs. TWI. (A-F) N = between 4 and 6 mice for each experimental group. Data are quantified as pg of PSY / μg of protein lysate, reported as mean ± SEM as a percentage vs. mean TWI cerebrum value, and compared using One way ANOVA (Bonferroni's test).

and kidneys were markedly lower compared to the nervous system, and exhibited no significant difference between TWI and TWI+RAPA (Fig. 3 E-F).

3.4. Rapamycin alleviates astrogliosis in TWI nervous system

In order to explore the therapeutic potential of RAPA in mitigating the physiopathological manifestations in TWI mice, we conducted an analysis focused on astrogliosis, a critical element in KD pathology [45]. Specifically, we quantified the expression of glial fibrillary acidic protein (GFAP), a predominant constituent of astrocytic cytoskeletal intermediate filaments, known to be upregulated in demyelinating disorders [51]. As previously documented by by our group and others [14,36,69,72], important astrogliosis was evident throughout the TWI mouse nervous system.

Utilizing immunohistochemistry, a conspicuous elevation in GFAP expression was discernible in the TWI brain compared to Wild-Type (WT) counterparts, as depicted in Fig. 4 A. This finding was corroborated by Western blot analyses, indicating augmented total GFAP levels in the brain, spinal cord, and sciatic nerves of TWI mice when compared to WT controls (Fig. 4 D). Notably, RAPA treatment could lead to a marked reduction in astrogliosis, as clear in the immunostaining presented in Fig. 4 A. Quantitative analysis of these images revealed a significant decrease in the number of astrocytes per image in TWI+RAPA mice compared to untreated TWI counterparts (P value <.001, TWI+RAPA vs. TWI; One-way ANOVA; Fig. 4 B). Additionally, the area occupied by astrocytes showed a declining trend between TWI+RAPA and TWI groups (P value <.05, TWI+RAPA vs. TWI; One-way ANOVA; Fig. 4 C).

Consistent with these findings, Western blot analyses indicated diminished total GFAP levels in TWI+RAPA mice compared to untreated TWI counterparts (P value <.05, TWI+RAPA vs. TWI; One-way ANOVA; Fig. 4 D). This reduction in total GFAP levels was also evident in the sciatic nerves and spinal cord of TWI+RAPA mice in comparison to TWI mice (Fig. 4 D), signifying a notable attenuation of astrogliosis mediated by RAPA in these organs. Remarkably, the reduction observed in the sciatic nerves and spinal cord was more pronounced than that in the brain (P value <.001, TWI-RAPA vs. TWI; One-way ANOVA).

Collectively, these results unequivocally indicate the presence of attenuated astrogliosis within the TWI nervous system mediated by RAPA treatment.

3.5. Limited impact of rapamycin treatment on TWI myelination

Finally, we explored the influence of RAPA on myelination, a critical facet of KD, wherein apoptosis of oligodendrocytes and Schwann cells represents the disease's primary pathology [24,62]. More specifically, we assessed the demyelination status by quantifying the expression of the myelin binding protein (MBP), a recognized myelin marker. Reduced expression of MBP is a common indicator associated with demyelinating diseases [30].

As expected, untreated TWI mice exhibited a reduction in total MBP levels in both the brain and spinal cord compared to WT counterparts (Fig. 5 B) [14,64]. Rapamycin treatment did not yield any discernible increase in total MBP content in TWI+RAPA mice relative to TWI controls (P value >.05, TWI+RAPA vs. TWI; One-way ANOVA). However, immunocytochemical staining indicated a modest preservation of myelin architecture, as evidenced by the noticeable increase in fluorescence emitted by MBP staining in TWI+RAPA mice compared to TWI (Fig. 5 B).

Additionally, our investigations revealed no significant effect of RAPA on enhancing the viability of primary GALC-deficient cells, supporting the hypothesis that RAPA does not markedly attenuate apoptosis in the context of GALC deficiency (Fig. S2).

In summary, our findings suggest a limited impact of RAPA treatment on myelination in TWI mice. Despite a subtle preservation of myelin architecture, the total MBP levels remained unaltered, emphasizing the challenges in modulating myelination dynamics in this disease

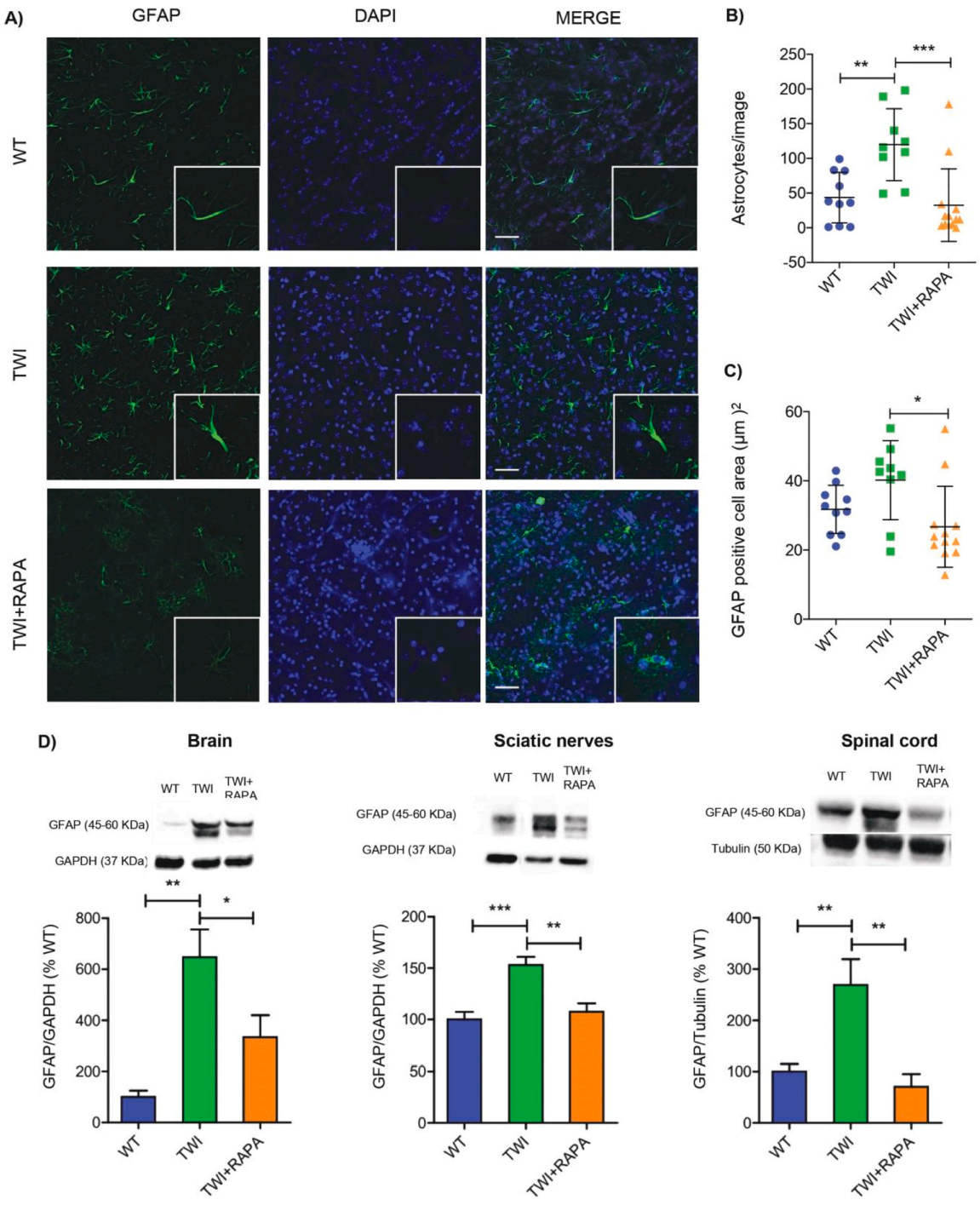

Fig. 4. Rapamycin treatment reduces astrogliosis in TWI mice. Immunohistochemistry staining of WT, TWI and TWI+RAPA brains with anti-GFAP (in green). Nuclei are stained with DAPI (in blue). A 6X zoom is showed in the right lower part of each merged image. Scale bar: 37 µm. B-C) Analysis of the number and average area of GFAP-stained astrocytes per imaging field. B) Number of astrocytes per image: *** P < 0.001, ** p < 0.01 TWI+RAPA vs. TWI, TWI vs. WT. (C) Average area of GFAP-stained astrocytes (µm2). * P < 0.05, TWI+RAPA vs. TWI. Data are reported as mean ± SD, and compared using One way ANOVA (Tukey's multiple comparisons test). N = between 9 and 13 images for each group. D) Western blot analysis of the total GFAP content in whole brain, sciatic nerves and spinal cord lysates of RAPA treated (TWI+RAPA) and untreated (WT, TWI) mice. Representative western blot bands are reported above each graph. N = between 4 and 6 mice for each experimental group. * P <.05, ** P <.01, *** P <.001 TWI vs. WT; TWI+RAPA vs. WT. data are reported as mean ± SEM, normalized to the total GAPDH content, reported as percentage vs. WT values, and compared using One way ANOVA (Bonferroni's test).

context.

4. Discussion

In this study, we investigated the effects of chronic Rapamycin (RAPA) administration in Twitcher (TWI) mice, a widely employed murine model for Krabbe Disease (KD). Characterized by an autosomal recessive mutation in the GALC gene leading to enzymatically inactive GALC enzyme, TWI mice exhibit pathology predominantly confined to the nervous system, closely mirroring the human condition [31].

The drug was administered ad libitum via drinking water at a concentration of 15 mg/L from PND 21–23. Starting administration at this

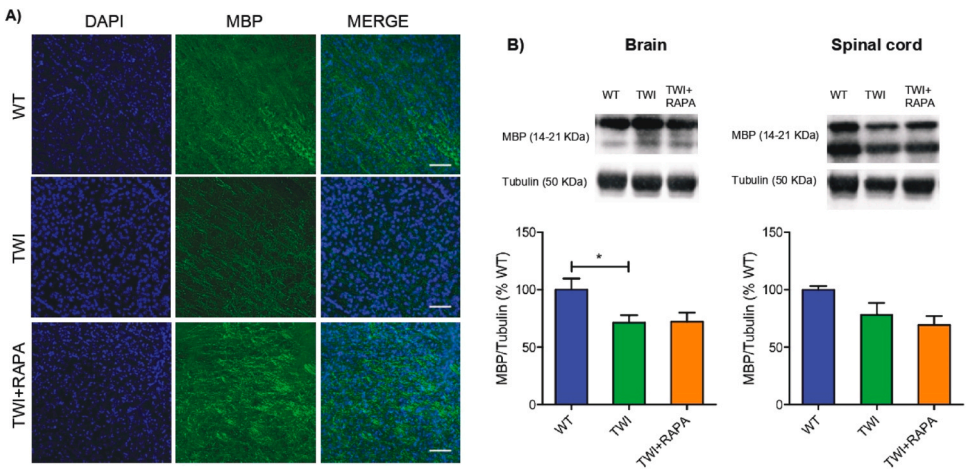

Fig. 5. Rapamycin treatment effect on TWI myelination. Immunohistochemistry staining of WT, TWI and TWI+RAPA brains with anti-MBP (in green). Nuclei are stained with DAPI (in blue). Scale bar: 37 μm. B) Western blot analysis of the total MBP content in whole brain, sciatic nerves and spinal cord lysates of RAPA treated (TWI+RAPA) and untreated (WT, TWI) mice. Representative western blot bands are reported above each graph. N = between 4 and 6 mice for each experimental group. * P <.05 TWI vs. WT. All data are reported as mean ± SEM, normalized to the total Tubulin content, reported as percentage vs. WT values, and compared using One way ANOVA (Bonferroni's test).

stage was strategic, aligning with the onset of symptoms in TWI mice [Duchen et al., 1980]. Clinically, this period holds significance as it coincides with the typical diagnosis of the disease, emphasizing its translational relevance [34,50]. This oral route was chosen to circumvent complications associated with repetitive injections, ensuring the well-being of the mice [70].

Given the pronounced motor impairments in TWI mice, we longitudinally monitored motor performance using grip strength and rotarod tests. Concurrently, we evaluated biochemical parameters linked to KD pathogenesis: PSY accumulation, astrogliosis, myelination, and autophagy markers.

Remarkably, we observed that RAPA temporarily enhances motor functions at specific stages of TWI mice development. Specifically, motor coordination, assessed via the rotarod test, improves significantly five days after treatment initiation (PND 24–25) but regresses to the untreated TWI mice levels during the advanced disease stages. In contrast, motor strength, evaluated through the hang wire test, shows improvement in RAPA-treated mice ten days post-treatment commencement (PND 29–30) but declines in the final observed time point (PND 35–37). These findings align with the progressive deterioration observed in TWI mouse body weight, a characteristic signifying disease progression [6,14]. Notably, RAPA administration did not adversely affect general mouse welfare parameters (i.e. food and water consumption, interaction with peers, normal respiration and provoked pattern of behavior, tremors, prostration, and self-mutilation), suggesting tolerance to the administered dose.

Subsequently, we investigated whether RAPA treatment induces autophagy in TWI mice. We observed increased conversion of LC3-I to LC3-II, indicating enhanced autophagy flux in both the central nervous system (CNS) (brain and spinal cord) and the peripheral nervous system (PNS) (sciatic nerve) of RAPA-treated mice. Additionally, we detected decreased total p62 levels in all tested organs of RAPA-treated mice and observed fewer p62 aggregates in brain slices from TWI+RAPA mice. Notably, the size of the p62 aggregates did not change in RAPA-treated mice compared to untreated mice, suggesting that RAPA treatment completely removes these aggregates rather than temporarily reducing their size.

These findings support the idea that RAPA may promote the clearance of p62-tagged protein aggregates, likely through p62/NBR1-mediated autophagosomal engulfment. Additionally, we observed the colocalization of p62 aggregates with Ubiquitin [33], consistent with previous reports [37]. Misfolded proteins, as described in the literature, often become polyubiquitylated, a modification that serves as a recognition signal for proteasomal degradation via the 26 S proteasome pathway. However, in cases where misfolded proteins aggregate, these structures are too large to enter 26 S proteasomes and are instead targeted for autophagic clearance, either through p62/NBR1-mediated autophagosomal engulfment or aggresome formation coordinated by HDAC6 [Kraft et al., 2010].

The reduction of p62 aggregates is an intriguing and promising finding from a translational clinical perspective. This aspect of KD is challenging to target with other GALC-deficiency correcting drugs, particularly in advanced disease stages.

Interestingly, Lin and colleagues recently demonstrated that repeated intraperitoneal injections of RAPA (3 mg/kg/day every 3 days) in TWI mice similarly reduce p62 aggregates in the brain [37]. However, they did not observe a decrease in the total p62 level in brain homogenates, which differs from our findings.

Furthermore, we observed that RAPA treatment significantly reduces astrogliosis in the TWI brain, spinal cord, and sciatic nerves compared to untreated TWI animals. This effect was confirmed through both immunohistochemistry on brain slices and western blot analysis of total brain, sciatic nerves, and spinal cord lysates. Consistent with our data, Lin and colleagues demonstrated that RAPA, using their administration protocol, alleviates astrocyte activation [37].

The reduction of astrogliosis is a particularly encouraging aspect of RAPA's effect on TWI mice from a clinical perspective. Extensive literature has highlighted the intrinsic link between astrogliosis and inflammation, driven by the role of inflammatory astrocytes and their interactions with other cells in the context of neuroinflammation [55]. Importantly, progressive inflammation in both the CNS and PNS is a prominent feature of KD, significantly contributing to KD pathogenesis, especially in the late disease stages [19,68].

Unfortunately, we did not observe substantial improvement in the myelination status in TWI mice treated with RAPA. Western blot analysis did not reveal any restoration of the total MBP level in TWI+RAPA mice compared to TWI mice. However, immunocytochemistry staining for MBP suggested some preservation of myelination architecture, consistent with recent findings by Lin and colleagues [37]. These data, along with our motor behavioral experiments, underscore the limited impact of this improvement on KD pathophysiology. Furthermore, we found no evidence of RAPA improving the cell viability of primary GALC-deficient cells, supporting the hypothesis that RAPA does not significantly enhance survival in a GALC-deficient condition.

Finally, we investigated RAPA's ability to promote PSY clearance in TWI tissues. Significant decreased PSY levels were observed in the spinal cord of TWI+RAPA mice, indicating that RAPA-mediated autophagy induction promotes PSY clearance in this organ. Conversely, no decrease was observed in other analyzed nervous system organs (cerebrum, cerebellum, and sciatic nerves).

We hypothesize that the varying permeabilities of biological barriers in different organs, such as the Blood Spinal Cord Barrier (BSCB) having higher permeability than the Blood Brain Barrier (BBB) [43], may contribute to these differential effects. BSCB's increased permeability could facilitate greater RAPA penetration into spinal cord cells, potentially enhancing PSY clearance. Notably, p62-aggregate clearance and GFAP reduction were higher in the spinal cord compared to the brain. While RAPA is known to cross the BBB, our results indicate that with the tested dose, the amount reaching the brain may be below the threshold required for effective PSY clearance. This aspect warrants meticulous evaluation to determine an optimal RAPA administration dose capable of promoting PSY clearance from the TWI brain and other organs.

The data presented in this study collectively demonstrate RAPA's capacity to improve crucial KD pathophysiological parameters, including PSY accumulation, protein aggregate abundance, and astrogliosis. These findings support the clinical translation of RAPA for KD treatment, especially given its existing use in clinical practice as an immunosuppressor (Sirolimus).

Notably, a clinical trial employing Sirolimus (RAPA) has been conducted for the treatment of amyotrophic lateral sclerosis (EudraCT Number: 2016–002399–28; ClinicalTrials.gov ID NCT03359538), a neurodegenerative disease sharing similarities with KD, such as neuromuscular dysfunctions [5]. Unfortunately, the results of this trial have not yet been published.

However, in our opinion, further studies are warranted to investigate RAPA's ability to promote PSY clearance. Optimizing the delivery route of RAPA to reach all desired organs with an effective drug dose would be invaluable. Exploring the encapsulation of RAPA [16,76] in biocompatible polymeric nanovectors [44], targeted specifically to organs such as the brain [13], offers a promising avenue for achieving this objective.

Fundings

This research was supported by the European Leukodystrophy Association (ELA) International, under the framework of the projects "Preclinical testing of single and combined autophagy modulation by Lithium and Rapamycin in Globoid Cell Leukodystrophy" (grant agreement no: 2018–008F2) and "nanoERT - Nanoparticle based Enzyme Replacement Therapy for the treatment of Krabbe disease: a pre-clinical study in the Twitcher Mouse" (grant agreement no: G.A. ELA n. 2019–008I2AV1 – NanoERT); by the European Molecular Biology Organization (EMBO) society, with the founding of a Travel-fellowship to participate at the 2023 EMBO workshop "RNA meets protein dacay"; by the BraYn association, with the founding of a Travel-fellowship to participate at the 2023 BraYn ("Brainstorming Research Assembly for Young Neuroscientists") conference.

CRediT authorship contribution statement

Lucia Angella: Methodology, Investigation, Data curation. **Husam B. R. Alabed:** Methodology, Investigation, Formal analysis. **Marco Cecchini:** Writing – review & editing, Writing – original draft, Supervision, Resources, Project administration, Investigation, Funding acquisition, Formal analysis, Data curation, Conceptualization. **Carla Emiliani:** Supervision, Resources, Data curation. **Ilaria Tonazzini:** Writing – review & editing, Methodology, Investigation. **Roberto Maria Pellegrino:** Methodology, Investigation, Formal analysis, Data curation. **Luca Scaccini:** Methodology, Investigation. **Miriam De Sarlo:** Writing – review & editing, Methodology, Investigation. **Sara Carpi:** Writing – review & editing, Methodology, Investigation, Formal analysis, Data curation. **Ambra Del Grosso:** Writing – review & editing, Writing – original draft, Methodology, Investigation, Funding acquisition, Formal analysis, Data curation, Conceptualization. **Laura Colagiorgio:** Methodology, Investigation.

Declaration of Competing Interest

The authors declare that they have no known competing financial interests or personal relationships that could have appeared to influence the work reported in this paper.

Data Availability

I have shared the link to my data set in the text of the manuscript

Acknowledgments

We thank Dr. Alessandra Biffi and Dr. Angela Gritti for giving us the heterozygous Twitcher mice, and European Leukodystrophy Association (ELA) International which supported this research (refer to the 'Funding' section for details).

Appendix A. Supporting information

Supplementary data associated with this article can be found in the online version at doi:10.1016/j.biopha.2024.116351. Dataset generated during the study are freely available on the ZENODO platform (https://zenodo.org/ accessed on 17 November 2023), at the following link https://zenodo.org/records/10040966 [15].

References

[1] H.B. Alabed, A. Del Grosso, V. Bellani, L. Urbanelli, S. Carpi, M. De Sarlo, R. M. Pellegrino, untargeted lipidomic approach for studying different nervous system tissues of the murine model of krabbe disease, Biomolecules 13 (10) (2023) 1562.
[2] M. Belleri, M. Presta, Endothelial cell dysfunction in globoid cell leukodystrophy, J. Neurosci. Res. 94 (11) (2016) 1359–1367.
[3] A.M. Bradbury, E.R. Bongarzone, M.S. Sands, Krabbe disease: new hope for an old disease, Neurosci. Lett. 752 (2021) 135841.
[4] S.P. Brooks, S.B. Dunnett, Tests to assess motor phenotype in mice: a user's guide, Nat. Rev. Neurosci. 10 (7) (2009) 519–529.
[5] Cantuti-Castelvetri, L., Maravilla, E., Marshall, M., Tamayo, T., D'auria, L., Monge, J.,. & Bongarzone, E.R. (2015). Mechanism of neuromuscular dysfunction in Krabbe disease. Journal of Neuroscience, 35(4), 1606-1616.
[6] S. Carpi, A. Del Grosso, M. De Sarlo, L. Colagiorgio, L. Scaccini, I. Tonazzini, M. Cecchini, Reliable and fast genotyping protocol for galactosylceramidase (Galc) in the twitcher (Twi) mouse, Biomedicines 10 (12) (2022) 3146.
[7] S. Carpi, A. Del Grosso, M. De Sarlo, L. Colagiorgio, L. Scaccini, I. Tonazzini, G. Parlanti, M. Cecchini, Data from: Reliable and fast genotyping protocol for galactosylceramidase (GALC) in the Twitcher (Twi) mouse, Dryad (2023), https://doi.org/10.5061/dryad.k3j9kd5br.
[8] M.A. Contreras, E. Haq, T. Uto, I. Singh, A.K. Singh, Psychosine-induced alterations in peroxisomes of twitcher mouse liver, Arch. Biochem. Biophys. 477 (2) (2008) 211–218.
[9] G. Dawson, Quantum dots and potential therapy for K rabbe's disease, J. Neurosci. Res. 94 (11) (2016) 1293–1303.
[10] A. Del Grosso, G. Parlanti, R. Mezzena, M. Cecchini, Current treatment options and novel nanotechnology-driven enzyme replacement strategies for lysosomal storage disorders, Adv. Drug Deliv. Rev. (2022) 114464.
[11] A. Del Grosso, S. Antonini, L. Angella, I. Tonazzini, G. Signore, M. Cecchini, Lithium improves cell viability in psychosine-treated MO3. 13 human oligodendrocyte cell line via autophagy activation, J. Neurosci. Res. 94 (11) (2016) 1246–1260.
[12] A. Del Grosso, L. Angella, I. Tonazzini, A. Moscardini, N. Giordano, M. Caleo, M. Cecchini, Dysregulated autophagy as a new aspect of the molecular pathogenesis of Krabbe disease, Neurobiol. Dis. *129* (2019) 195–207.
[13] A. Del Grosso, M. Galliani, L. Angella, M. Santi, I. Tonazzini, G. Parlanti, M. Cecchini, Brain-targeted enzyme-loaded nanoparticles: A breach through the blood-brain barrier for enzyme replacement therapy in Krabbe disease, Sci. Adv. 5 (11) (2019) eaax7462.
[14] Del Grosso, A., Parlanti, G., Angella, L., Giordano, N., Tonazzini, I., Ottalagana, E.,. & Cecchini, M. (2022). Chronic lithium administration in a mouse model for Krabbe disease. *JIMD reports*, *63*(1), 50-65.
[15] Del Grosso, A., Carpi, S., De Sarlo, M., Scaccini, L., Colagiorgio, L., Alabed, H.B.R.,. & Cecchini, M. (2023) Data From: Chronic Rapamycin Administration via Drinking Water Mitigates the Pathological Phenotype in a Krabbe Disease Mouse Model

Through Autophagy Activation. Zenodo. DOI: https://zenodo.org/records/10040966.
[16] L.R. Dos Reis, M.T. Luiz, R.M. Sábio, G.D. Marena, D. Filippo, J.L. Duarte, L. S. Fernandes, V.H. Sousa Araújo, V.A. Oliveira Silva, M. Chorilli, Design of rapamycin and resveratrol coloaded liposomal formulation for breast cancer therapy, Nanomed. 10 (2023) 789–801.
[17] L.W. Duchen, E.M. Eicher, J.M. Jacobs, F. Scaravilli, F. Teixeira, Hereditary leucodystrophy in the mouse: the new mutant twitcher, Brain: a journal of neurology 103 (3) (1980) 695–710.
[18] M.L. Escolar, M.D. Poe, J.M. Provenzale, K.C. Richards, J. Allison, S. Wood, J. Kurtzberg, Transplantation of umbilical-cord blood in babies with infantile Krabbe's disease, N. Engl. J. Med. 352 (20) (2005) 2069–2081.
[19] M.L. Feltri, N.I. Weinstock, J. Favret, N. Dhimal, L. Wrabetz, D. Shin, Mechanisms of demyelination and neurodegeneration in globoid cell leukodystrophy, Glia 69 (10) (2021) 2309–2331.
[20] A.M. Floden, C.K. Combs, Microglia demonstrate age-dependent interaction with amyloid-β fibrils, J. Alzheimer'S. Dis. 25 (2) (2011) 279–293.
[21] R. Fu, Q. Mei, W. Zuo, J. Li, D. Gregor, A. Bekker, J. Ye, Low-dose ethanol excites lateral habenula neurons projecting to VTA, RMTg, and raphe, Int. J. Physiol., Pathophysiol. Pharmacol. 9 (6) (2017) 217.
[22] M. Fuller, J. Szer, S. Stark, J.M. Fletcher, Rapid, single-phase extraction of glucosylsphingosine from plasma: a universal screening and monitoring tool, Clin. Chim. Acta 450 (2015) 6–10.
[23] M. Galliani, M. Santi, A. Del Grosso, A. Cecchettini, F.M. Santorelli, S.L. Hofmann, G. Signore, Cross-Linked enzyme aggregates as versatile tool for enzyme delivery: application to polymeric nanoparticles, Bioconjugate Chem. 29 (7) (2018) 2225–2231.
[24] A.C.E. Graziano, V. Cardile, History, genetic, and recent advances on Krabbe disease, Gene 555 (1) (2015) 2–13.
[25] J.A. Hawkins-Salsbury, A.R. Parameswar, X. Jiang, P.H. Schlesinger, E. Bongarzone, D.S. Ory, M.S. Sands, Psychosine, the cytotoxic sphingolipid that accumulates in globoid cell leukodystrophy, alters membrane architecture, J. Lipid Res. 54 (12) (2013) 3303–3311, https://doi.org/10.1194/jlr.M039610 [PubMed: 24006512].
[26] Heller, G.J., Marshall, M.S., Issa, Y., Marshall, J.N., Nguyen, D., Rue, E.,. & Bongarzone, E.R. (2021). Waning efficacy in a long-term AAV-mediated gene therapy study in the murine model of Krabbe disease. Molecular Therapy, 29(5), 1883-1902.
[27] C.H. Hill, S.C. Graham, R.J. Read, J.E. Deane, Structural snapshots illustrate the catalytic cycle of β-galactocerebrosidase, the defective enzyme in Krabbe disease, Proc. Natl. Acad. Sci. 110 (51) (2013) 20479–20484.
[28] S. Huber, C.J. Bruns, G. Schmid, P.C. Hermann, C. Conrad, H. Niess, M. Guba, Inhibition of the mammalian target of rapamycin impedes lymphangiogenesis, Kidney Int. 71 (8) (2007) 771–777.
[29] T. Ichioka, Y. Kishimoto, S. Brennan, G.W. Santos, A.M. Yeager, Hematopoietic cell transplantation in murine globoid cell leukodystrophy (the twitcher mouse): effects on levels of galactosylceramidase, psychosine, and galactocerebrosides, Proc. Natl. Acad. Sci. 84 (12) (1987) 4259–4263.
[30] M. Khodanovich, A. Pishchelko, V. Glazacheva, E. Pan, A. Akulov, M. Svetlik, V. Yarnykh, Quantitative imaging of white and gray matter remyelination in the cuprizone demyelination model using the macromolecular proton fraction, Cells 8 (10) (2019) 1204.
[31] T. Kobayashi, T. Yamanaka, J.M. Jacobs, F. Teixeira, K. Suzuki, The Twitcher mouse: an enzymatically authentic model of human globoid cell leukodystrophy (Krabbe disease), Brain Res. 202 (2) (1980) 479–483.
[32] Koelmel, J.P., Li, X., Stow, S.M., Sartain, M.J., Murali, A., Kemperman, R.,. & Kitagawa, N. (2020). Lipid annotator: towards accurate annotation in non-targeted liquid chromatography high-resolution tandem mass spectrometry (LC-HRMS/MS) lipidomics using a rapid and user-friendly software. Metabolites, 10(3), 101.
[33] E.A. Komarova, M.P. Antoch, L.R. Novototskaya, O.B. Chernova, G. Paszkiewicz, Leontieva, C. Kraft, M. Peter, K. Hofmann, Selective autophagy: ubiquitin-mediated recognition and beyond, Nat. Cell Biol. 12 (9) (2010) 836–841.
[34] J.M. Kwon, D. Matern, J. Kurtzberg, L. Wrabetz, M.H. Gelb, D.A. Wenger, J. J. Orsini, Consensus guidelines for newborn screening, diagnosis and treatment of infantile Krabbe disease, Orphanet J. Rare Dis. 13 (1) (2018) 1–10.
[35] O.V. Leontieva, G.M. Paszkiewicz, M.V. Blagosklonny, Comparison of rapamycin schedules in mice on high-fat diet, Cell Cycle 13 (21) (2014) 3350–3356.
[36] D.S. Lin, C.S. Ho, Y.W. Huang, T.Y. Wu, T.H. Lee, Z.D. Huang, M.F. Chiang, Impairment of proteasome and autophagy underlying the pathogenesis of leukodystrophy, Cells 9 (5) (2020) 1124.
[37] D.S. Lin, Y.W. Huang, T.H. Lee, L. Chang, Z.D. Huang, T.Y. Wu, C.S. Ho, Rapamycin alleviates protein aggregates, reduces neuroinflammation, and rescues demyelination in globoid cell leukodystrophy, Cells 12 (7) (2023) 993.
[38] Y. Lu, B. Lin, J. Zhong, The therapeutic effect of dexmedetomidine on rat diabetic neuropathy pain and the mechanism, Biol. Pharm. Bull. 40 (9) (2017) 1432–1438.
[39] M.S. Marshall, Y. Issa, B. Jakubauskas, M. Stoskute, V. Elackattu, J.N. Marshall, E. R. Bongarzone, Long-term improvement of neurological signs and metabolic dysfunction in a mouse model of Krabbe's disease after global gene therapy, Mol. Ther. 26 (3) (2018) 874–889.
[40] R. Mezzena, A. Del Grosso, R.M. Pellegrino, H.B. Alabed, C. Emiliani, I. Tonazzini, M. Cecchini, Mechanotransduction Impairment in Primary Fibroblast Model of Krabbe Disease, Biomedicines 11 (3) (2023) 927.
[41] C.R. Mikulka, M.S. Sands, Treatment for Krabbe's disease: Finding the combination, J. Neurosci. Res. 94 (11) (2016) 1126–1137.
[42] N. Mizushima, T. Yoshimori, How to interpret LC3 immunoblotting, Autophagy *3* (6) (2007) 542–545.
[43] K. Montague-Cardoso, M. Malcangio, Changes in blood–spinal cord barrier permeability and neuroimmune interactions in the underlying mechanisms of chronic pain, Pain. Rep. 6 (1) (2021).
[44] Narmani, A., Jahedi, R., Bakhshian-Dehkordi, E., Ganji, S., Nemati, M., Ghahramani-Asl, R.,. & Sahebkar, A. (2023). Biomedical applications of PLGA nanoparticles in nanomedicine: Advances in drug delivery systems and cancer therapy. Expert Opinion on Drug Delivery, (just-accepted).
[45] A.M. Nicaise, E.R. Bongarzone, S.J. Crocker, A microglial hypothesis of globoid cell leukodystrophy pathology, J. Neurosci. Res. 94 (11) (2016) 1049–1061.
[46] O. V., & Gudkov, A.V. (2012). Rapamycin extends lifespan and delays tumorigenesis in Pathological Society of Great Britain and Ireland, 219(1), 35-40.
[47] K.M. Page, E.O. Stenger, J.A. Connelly, D. Shyr, T. West, S. Wood, J. Kurtzberg, Hematopoietic stem cell transplantation to treat leukodystrophies: clinical practice guidelines from the Hunter's Hope Leukodystrophy Care Network, Biol. Blood Marrow Transplant. 25 (12) (2019) e363–e374.
[48] N. Papini, R. Todisco, P. Giussani, M. Dei Cas, R. Paroni, C. Giallanza, C. Tringali, Impaired autophagy in krabbe disease: the role of BCL2 and beclin-1 phosphorylation, Int. J. Mol. Sci. 24 (6) (2023) 5984.
[49] D. Pellegrini, A. Del Grosso, L. Angella, N. Giordano, M. Dilillo, I. Tonazzini, L. A. McDonnell, quantitative microproteomics based characterization of the central and peripheral nervous system of a mouse model of krabbe disease*[S], Mol. Cell. Proteom. 18 (6) (2019) 1227–1241.
[50] S. Pike-Langenfeld, Why must the debate continue on Krabbe disease newborn screening? (June), in: American Journal of Medical Genetics Part C: Seminars in Medical Genetics, Vol. 190 John Wiley & Sons, Inc, Hoboken, USA, 2022, pp. 153–155 (June).
[51] B.F.G. Popescu, C.F. Lucchinetti, Pathology of demyelinating diseases. Annual Review of Pathology: Mechanisms of Disease 7 (2012) 185–217.
[52] M.A. Rafi, H.Z. Rao, P. Luzi, A. Luddi, M.T. Curtis, D.A. Wenger, Intravenous injection of AAVrh10-GALC after the neonatal period in twitcher mice results in significant expression in the central and peripheral nervous systems and improvement of clinical features, Mol. Genet. Metab. 114 (3) (2015) 459–466.
[53] B. Ravikumar, S. Sarkar, J.E. Davies, M. Futter, M. Garcia-Arencibia, Z.W. Green-Thompson, D.C. Rubinsztein, Regulation of mammalian autophagy in physiology and pathophysiology, Physiol. Rev. 90 (4) (2010) 1383–1435.
[54] R. Rebiai, E. Rue, S. Zaldua, D. Nguyen, G. Scesa, M. Jastrzebski, E.R. Bongarzone, CRISPR-Cas9 Knock-In of T513M and G41S mutations in the murine β–galactosyl-ceramidase gene re-capitulates early-onset and adult-onset forms of krabbe disease, Front. Mol. Neurosci. 15 (2022).
[55] J.K. Reid, H.F. Kuipers, She doesn't even go here: the role of inflammatory astrocytes in CNS disorders, Front. Cell. Neurosci. 15 (2021) 704884.
[56] J.J. Ribbens, A.B. Moser, W.C. Hubbard, E.R. Bongarzone, G.H. Maegawa, Characterization and application of a disease-cell model for a neurodegenerative lysosomal disease, Mol. Genet. Metab. 111 (2) (2014) 172–183.
[57] A. Ricca, A. Gritti, Perspective on innovative therapies for globoid cell leukodystrophy, J. Neurosci. Res. 94 (11) (2016) 1304–1317.
[58] A. Ricca, N. Rufo, S. Ungari, F. Morena, S. Martino, W. Kulik, A. Gritti, Combined gene/cell therapies provide long-term and pervasive rescue of multiple pathological symptoms in a murine model of globoid cell leukodystrophy, Hum. Mol. Genet. 24 (12) (2015) 3372–3389.
[59] M. Righi, G.L. Puleo, I. Tonazzini, G. Giudetti, M. Cecchini, S. Micera, Peptide-based coatings for flexible implantable neural interfaces, Sci. Rep. 8 (1) (2018) 502.
[60] J. Robinson, C. Lai, A. Martin, E. Nye, I. Tomlinson, A. Silver, Oral rapamycin reduces tumour burden and vascularization in Lkb1+/− mice, J. Pathol.: A J. Pathol. Soc. Gt. Br. Irel. 219 (1) (2009) 35–40.
[61] A. Safary, M.A. Khiavi, R. Mousavi, J. Barar, M.A. Rafi, Enzyme replacement therapies: what is the best option? BioImpacts: BI 8 (3) (2018) 153.
[62] N. Sakai, Pathogenesis of leukodystrophy for Krabbe disease: molecular mechanism and clinical treatment, Brain Dev. 31 (7) (2009) 485–487.
[63] S.E. Siegmund, H. Yang, R. Sharma, M. Javors, O. Skinner, V. Mootha, E.A. Schon, Low-dose rapamycin extends lifespan in a mouse model of mtDNA depletion syndrome, Hum. Mol. Genet. 26 (23) (2017) 4588–4605.
[64] B. Smith, F. Galbiati, L.C. Castelvetri, M.I. Givogri, A. Lopez-Rosas, E. R. Bongarzone, Peripheral neuropathy in the Twitcher mouse involves the activation of axonal caspase 3, ASN Neuro *3* (4) (2011) AN20110019.
[65] B.R. Smith, M.B. Santos, M.S. Marshall, L. Cantuti-Castelvetri, A. Lopez-Rosas, G. Li, E.R. Bongarzone, Neuronal inclusions of α-synuclein contribute to the pathogenesis of Krabbe disease, J. Pathol. 232 (5) (2014) 509–521.
[66] C. Spalletti, C. Alia, S. Lai, A. Panarese, S. Conti, S. Micera, M. Caleo, Combining robotic training and inactivation of the healthy hemisphere restores pre-stroke motor patterns in mice, Elife 6 (2017) e28662.
[67] S. Spassieva, E. Bieberich, Lysosphingolipids and sphingolipidoses: psychosine in Krabbe's disease, J. Neurosci. Res. 94 (11) (2016) 974–981.
[68] H. Takahashi, K. Suzuki, Globoid cell leukodystrophy: Specialized contact of globoid cell with astrocyte in the brain of twitcher mouse, Acta Neuropathol. 58 (4) (1982) 237–242.
[69] I. Tonazzini, C. Cerri, A. Del Grosso, S. Antonini, M. Allegra, M. Caleo, M. Cecchini, Visual system impairment in a mouse model of Krabbe disease: the Twitcher mouse, Biomolecules *11* (1) (2020) 7.
[70] P.V. Turner, T. Brabb, C. Pekow, M.A. Vasbinder, Administration of substances to laboratory animals: routes of administration and factors to consider, J. Am. Assoc. Lab. Anim. Sci. 50 (5) (2011) 600–613.
[71] E. Vannini, F. Maltese, F. Olimpico, A. Fabbri, M. Costa, M. Caleo, L. Baroncelli, Progression of motor deficits in glioma-bearing mice: Impact of CNF1 therapy at symptomatic stages, Oncotarget 8 (14) (2017) 23539.

[72] N.I. Weinstock, C. Kreher, J. Favret, D. Nguyen, E.R. Bongarzone, L. Wrabetz, D. Shin, Brainstem development requires galactosylceramidase and is critical for pathogenesis in a model of Krabbe disease, Nat. Commun. 11 (1) (2020) 5356.
[73] D.A. Wenger, M.A. Rafi, P. Luzi, J. Datto, E. Costantino-Ceccarini, Krabbe disease: genetic aspects and progress toward therapy, Mol. Genet. Metab. 70 (1) (2000) 1–9.
[74] A.B. White, M.I. Givogri, A. Lopez-Rosas, H. Cao, R. van Breemen, G. Thinakaran, E.R. Bongarzone, Psychosine accumulates in membrane microdomains in the brain of krabbe patients, disrupting the raft architecture, J. Neurosci. 29 (19) (2009) 6068–6077.
[75] M. Zaka, D.A. Wenger, Psychosine-induced apoptosis in a mouse oligodendrocyte progenitor cell line is mediated by caspase activation, Neurosci. Lett. 358 (3) (2004) 205–209.
[76] Q. Zhou, J.D. Quirk, Y. Hu, H. Yan, J.P. Gaut, C.T. Pham, H. Pan, Rapamycin perfluorocarbon nanoparticle mitigates cisplatin-induced acute kidney injury, Int. J. Mol. Sci. 24 (7) (2023) 6086.